AIP Journal of Applied Physics

Morphologically manipulated Ag/ZnO nanostructures as surface enhanced Raman scattering probes for explosives detection

Ummar Pasha Shaik, Syed Hamad, Md. Ahamad Mohiddon, Venugopal Rao Soma, and M. Ghanashyam Krishna

Citation: Journal of Applied Physics **119**, 093103 (2016); doi: 10.1063/1.4943034
View online: http://dx.doi.org/10.1063/1.4943034
View Table of Contents: http://scitation.aip.org/content/aip/journal/jap/119/9?ver=pdfcov
Published by the AIP Publishing

Morphologically manipulated Ag/ZnO nanostructures as surface enhanced Raman scattering probes for explosives detection

Ummar Pasha Shaik,[1] Syed Hamad,[2] Md. Ahamad Mohiddon,[3,a)] Venugopal Rao Soma,[1] and M. Ghanashyam Krishna[1,2,4]
[1]*Advanced Center of Research in High Energy Materials (ACRHEM), University of Hyderabad, Hyderabad, Telangana 500046, India*
[2]*School of Physics, University of Hyderabad, Hyderabad, Telangana 500046, India*
[3]*Department of Science and Humanities, National Institute of Technology Andhra Pradesh, Tadepalligudem 534101, India*
[4]*Centre for Advanced Studies in Electronics Science and Technology, School of Physics, University of Hyderabad, Hyderabad, Telangana 500046, India*

(Received 8 November 2015; accepted 13 February 2016; published online 4 March 2016)

The detection of secondary explosive molecules (e.g., ANTA, FOX-7, and CL-20) using Ag decorated ZnO nanostructures as surface enhanced Raman scattering (SERS) probes is demonstrated. ZnO nanostructures were grown on borosilicate glass substrates by rapid thermal oxidation of metallic Zn films at 500 °C. The oxide nanostructures, including nanosheets and nanowires, emerged over the surface of the Zn film leaving behind the metal residue. We demonstrate that SERS measurements with concentrations as low as 10 μM, of the three explosive molecules ANTA, FOX-7, and CL-20 over ZnO/Ag nanostructures, resulted in enhancement factors of $\sim 10^7$, $\sim 10^7$, and $\sim 10^4$, respectively. These measurements validate the high sensitivity of detection of explosive molecules using Ag decorated ZnO nanostructures as SERS substrates. The Zn metal residue and conditions of annealing play an important role in determining the detection sensitivity. © *2016 AIP Publishing LLC*.
[http://dx.doi.org/10.1063/1.4943034]

I. INTRODUCTION

Detection of explosives, such as RDX (cyclotrimethylenetrinitramine), trinitrotoluene (TNT), dinitrotoluene (DNT), and ammonium nitrate (AN), in low concentrations is an extremely important area of basic and applied research in the context of security. Over the last few years, research in this area has focused on detection of trace quantities of explosives for which numerous strategies have been developed.[1–3] One class of techniques that is rapidly emerging as a reliable and fast route to detect explosives is based on Surfaced Enhanced Raman Scattering (SERS).[3–5] This is due to the fact that the extremely strong local electric field concentrated at the metal dielectric interface has a profound impact on the Raman scattering cross-sections, which in turn enables molecular identification and sensing applications at the trace level.[6–10] It is well documented that noble metal (Au, Ag, and Cu) nanoparticles exhibit strong surface plasmons resonances (SPR) in the UV-Visible region of the electromagnetic spectrum. Absorption, scattering cross sections, and, therefore, SPR behaviour can be tuned by a variety of parameters such as metal nanoparticle dimensions, geometry, and dielectric constant of the medium in which they are embedded.[6–9] When the spatial gap between the metal nanoparticles is brought down, the electric field confined over it undergoes a strong coupling which results in a "hot spot" leading to novel applications in photovoltaics, SERS, nonlinear optics, surface enhanced fluorescence, and chemical sensing. Thus, the combined effect of giant electric field of the plasmonic hot spot and a chemical charge transfer effect results in the enhancement of the Raman scattering signal on surfaces on which these metal nanoparticles exist. Apart from noble metal nanoparticle surfaces, noble metal particle decorated nanostructures have also been found to be attractive as SERS substrates.[11–13] Rajh and co-workers have reported that the semiconductor nanoparticles demonstrated SERS enhancement of $\sim 10^3$ times, due to the hybrid charge transfer (CT) system.[14] By combining the contributions from electromagnetic enhancement and semiconductor induced CT enhancement in metal/semiconductor nanostructure, it is expected to achieve large enhancements in these hybrid nanostructures. In addition to the above mentioned reason, the surface morphology of the nanostructure could also affect the SERS enhancement. Nanostructures such as nanorods or nanosheets are proposed as promising SERS substrates; due to their lightning, rod type morphology produces more "hot spots" for stronger local electric fields and promotes the SERS enhancement.[13,15] Ag decorated ZnO nanostructures (such as nanowires and nanosheets) are one such class of structures investigated for application in biosensors, electric devices, photocatalytic cells, photo-detectors, and gas sensing.[11–13,16–18] ZnO with a direct band gap of 3.37 eV and large excitation binding energy of 60 meV offers a good choice of semiconductor material as a SERS active substrate.[10,19–21] The enhanced light absorption in a semiconductor when the plasmon resonance energy overlap with the band gap absorption of the semiconductor and electron–hole separation (through transfer of the energetic electrons between the metal and the semiconductor) are expected to

a)Email: ahamed.vza@gmail.com. Telephone: 91-40-23134382. FAX: 91-40-23010227.

play major role in obtaining large SERS enhancements. Recently, several groups have reported that these 3D morphologies decorated by noble metal nanoparticles can improve the sensitivity of molecular detection in various SERS applications.[11–13,18,22,23] The feasibility of synthesizing different ZnO morphologies with high surface-to-volume ratios, such as nanowires,[24] nano-flowers, and nano-tetrapods, makes it an ideal candidate for studying morphology aided SERS studies. Kang *et al*. developed a photo-induced synthesis method for fabricating metal nanoparticles (NPs) embedded on the surfaces of ZnO nanowires to form hierarchical nanostructures and presented the SERS application in determining the glucose concentration.[25] He *et al*. presented a simple and green strategy to fabricate Ag-decorated ZnO nanorod arrays based on electrophoretic deposition in Ag colloidal solution prepared by laser ablation in water.[26] Tao *et al*. reported the growth of flowers like Ag decorated ZnO nanorods produced on patterned sapphire substrate and presented its SERS application by Rh6G probing molecule.[27] Zu *et al*. described a sacrificial template synthetic approach for the fabrication of the arrays of Ag-Au-Pd-Pt/ZnO-nanotaper and presented its SERS application by Rh6G.[28] However, there are very few reports on the use of Ag decorated ZnO nanowires for explosive detection.[29] SERS technique for explosives detection is in the nascent stages, and several approaches have been investigated by several research groups all over the world, including our own, due to its superior performance compared to other techniques.[3] Hakonen *et al*. has reviewed the recent SERS substrates utilized for explosives detection and emphasized the importance of investigating novel substrates and methodologies for efficient detection of a variety of explosive molecules.[3] Therefore, in this work, we have investigated the potential of Ag decorated ZnO nanowires as SERS substrate for explosive detection by studying different morphologies achieved through varied growth conditions. The ZnO nanowires are fabricated by single step thermal oxidation of Zn metal films as reported by some of the current authors.[24] The ZnO nanowires are decorated with Ag nanoparticles by low energy ion beam sputter deposition. The SERS signal from the Ag decorated ZnO nanowires was thoroughly scrutinized for understanding the detection mechanism of 5-amiano-3-nitro-1 H-1,2,4-triazole (ANTA), 1,1-diamino-2,2 dinitroethene (FOX-7), and 2,4,6,8,10,12-hexanitro-2,4,6,8,10,12-hexaazaisowurtzitane (CL-20) explosive molecules without functionalizing the surface.

II. EXPERIMENTAL DETAILS

The detailed experimental procedure is schematically illustrated in Fig. 1. Zn metal film of 1500 nm thickness was deposited on a borosilicate glass (BSG) substrate [Fig. 1(a)] by thermal evaporation using high purity Zn metal granules (Aldrich, 99.99%). The source to substrate separation was fixed at 10 cm, and the substrates were maintained at ambient temperature during deposition. The as-deposited metal Zn films [Fig. 1(b)] were loaded into a furnace preheated to a temperature of 500 °C and maintained at this temperature for dwell times of 5, 10, 15, 20, 25, and 30 min (Morphology A, B, C, D, E, and F, respectively). The furnace was then switched off and allowed to return to room temperature. This resulted in the formation of various complex nanostructures of Zn/ZnO with different metal residue [Fig. 1(c)]. Further details of deposition and annealing treatments are described in our previous work.[24,30,31] These nanostructures were decorated with Ag nanoparticles deposited by ion beam sputter deposition [Fig. 1(d)] using a Kaufman type ion source (DC25 of Oxford Applied Research, UK) with argon ions of energy 400 eV and beam currents of 9 mA bombarding the Ag (99.99% purity) target. The Ag target-substrate distance was >10 cms. The combination of low energy, low flux, and large substrate distances resulted in extremely good control

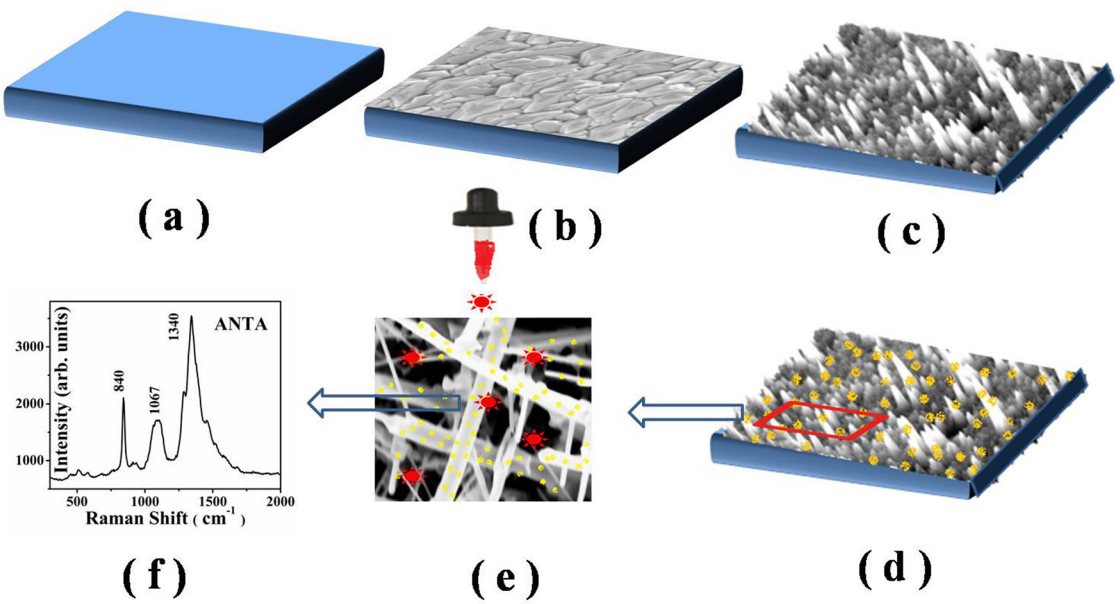

FIG. 1. Schematic representation of experimental procedure for preparing ZnO films: (a) BSG substrate; (b) 1500 nm Zn film deposited by thermal evaporation; (c) ZnO nanostructure, after subjecting a rapid annealing at 500 °C; (d) Ag nanoparticles decorated on ZnO nanostructure; (e) SEM image of a selected region of Fig. 1(d) along with analyte detection; (f) Raman spectra of the detected analyte (ANTA).

over the microstructural evolution of the Ag films.[32] The Ag deposition was carried out at a rate of 1 nm/min to obtain thin films of approximately 10 nm thickness. The Ag film was deposited simultaneously on the BSG substrate coated with ZnO nanostructures as well as the bare substrate under the same deposition conditions. The BSG/ZnO/Ag nanostructures are referred to as Ag decorated ZnO nanostructures and ZnO/Ag in the rest of the paper. The BSG/Ag nanostructure has been used as a reference to compare the enhancement of SERS signal recorded over BSG/ZnO/Ag nanostructure. The film thickness was measured after deposition using a surface profilometer (model XP-1 Ambios Tech., USA). The presence of metal residue in the annealed Zn film was confirmed by X-ray diffraction patterns recorded in a powder X-ray diffractometer (Discover D8 diffractometer of Bruker, Germany) with Cu K_α radiation (wavelength = 0.15408 nm). The surface morphology was examined under a field emission scanning electron microscope (FE-SEM) (Model Ultra55 of Carl Zeiss, Germany) equipped with an energy dispersive X-ray spectrometer (EDS) (of Oxford instruments INCA-Xact, UK) to determine the elemental characterization of the nanostructures. Transmission electron microscopy study was carried out by a Tecnai 20 G2 STwin, FEI electron microscope, operated at 200 kV. SERS experiments were performed in a confocal mirco-Raman spectrometer (Alpha 300 of Witec, Germany) equipped with a second harmonic Nd-YAG laser excitation source of 532 nm wavelength. The following conditions were maintained for all the SERS experiments; minimum power, 100× objective, integration time of 1 s, and all other instrument optics. A drop of liquid (typically 10 μl volume) was pipetted out on to the ZnO/Ag surface to form a thin layer of explosive molecule under investigation [Fig. 1(e)]. Raman spectra were collected at different points on the surface, and the average of five spectra has been used as a reference for comparison in the analysis [Fig. 1(f)]. All the ZnO nanostructures decorated with Ag were investigated with Rhodamine 6 G (Rh6G) as the control sample followed by the explosive molecules of ANTA, FOX-7, and CL-20.

III. RESULTS AND DISCUSSION

The as-deposited Zn metal film has highly dense, crack free, and triangular grain morphology, as observed in our previous studies.[33] Different microstructures were achieved by varying annealing treatment procedure, and the obtained structures are illustrated in Figures 2(a)–2(f), along with the morphology of the Ag decorated ZnO film in the inset of Fig. 2(c). The morphology A of the Zn film in Fig. 2(a) depicts smearing of the grain boundaries indicating the onset of grain melting. A completely transformed grain shape was evidenced for morphology B of Zn film in Fig. 2(b), indicating the complete melting of the as-deposited film surface. The microstructures of the morphologies C to F comprised ZnO nanowires of diameter 10–200 nm and length of few μm [Figs. 2(c)–2(f)]. Additional detailed information about the morphology was extracted from atomic force microscopy (AFM) measurements of the above samples. The diverse microstructure of ZnO films achieved by subjecting the metallic Zn films to different annealing treatments is presented in Figures 3(a)–3(f). The line profile across the horizontal direction of about 20 μm length on each AFM image is presented in the supplementary material S1.[34] Morphology A in Fig. 3(a) shows uniform spherical grain distribution across the surface of the film. The line profile shows maximum peak to peak height (PPH) of 130 nm. Morphology B, shown in Fig. 3(b), has mixed regions of smooth morphology and rough surface comprised distorted spherical grains of

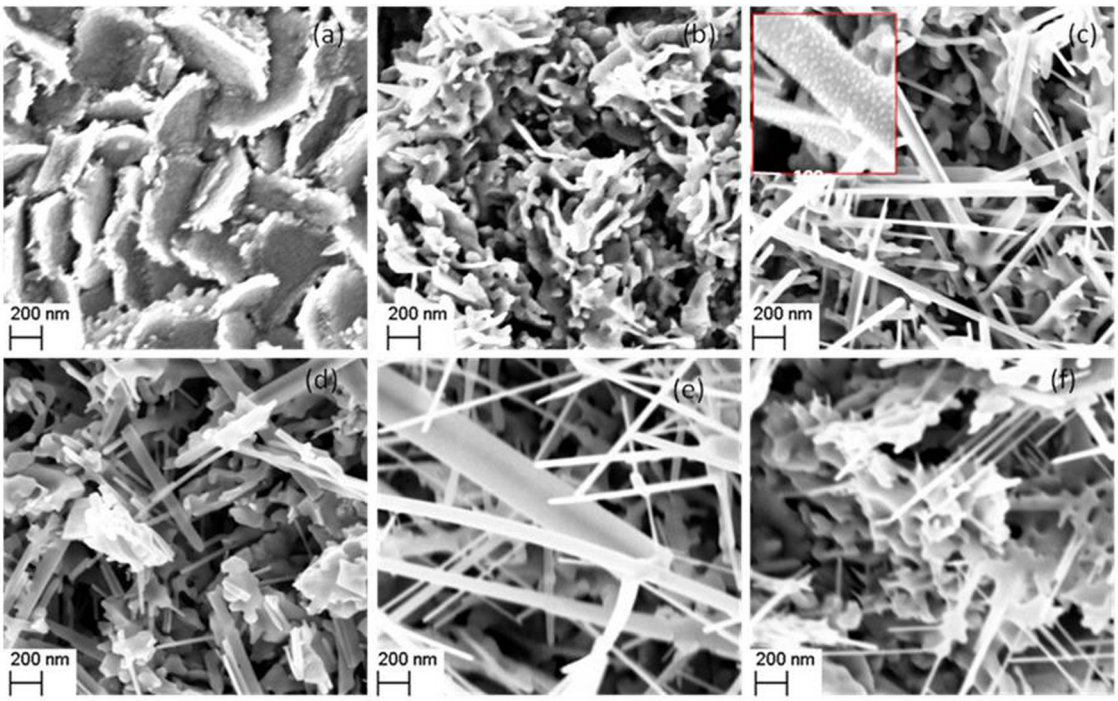

FIG. 2. FESEM images of Zn films annealed at 500 °C for different morphologies A (a); B (b); C (c); D (d); E (e), and F (f).

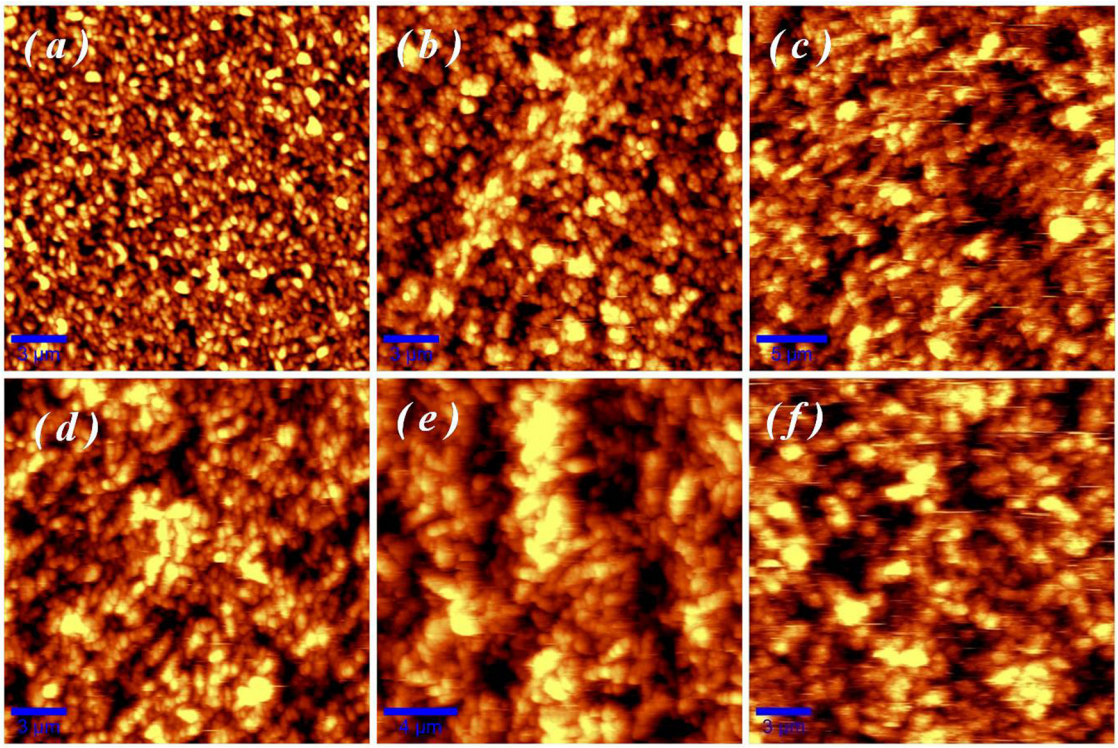

FIG. 3. Atomic force micrographs of Zn films annealed at 500 °C for different morphologies A (a); B (b); C (c); D (d); E (e), and F (f).

varying dimensions with a PPH of 180 nm. Morphology C has completely lost the smooth spherical grain regions, and relatively elongated grains of diverse dimensions are grown as observed in Fig. 3(c). A similar morphological flip is evident in the FESEM images of Morphology C sample. This is accompanied by a rise in the PPH value to 520 nm. Further roughening of the surface is evidenced in the morphology D with a PPH of 620 nm. The enhanced elongation in grain shape is attributed to the presence of nanorods observed in FESEM images. A completely different morphology with high roughness and PPH value of 1420 nm is observed in the morphology E. The microstructure has separated fringes like structures along with the highly rough region spread over each fringe. Large nanorods with no residual grains, observed in FESEM image, of morphology E are expected to be the reason behind such fringe like structure. Morphology F is much similar like Morphology D with almost same peak to peak cross sectional roughness. Further characterizations of the ZnO nanostructures have been carried out by XRD, Raman spectroscopy, and TEM, and are depicted in Fig. 4. The XRD pattern of two BSG/Zn films, as-deposited and morphology C samples, are compared in Fig. 4(a). The as-deposited film has a diffraction pattern wherein all the peaks can be assigned to hexagonal metallic Zn (indexed according to JCPDS No 87–0713). No signature of oxidation is recorded in the as-deposited film. The BSG/Zn film morphology C exhibits a set of XRD peaks, which are different from those observed in the diffraction pattern of as-deposited film (metallic Zn peaks are designated by asterisk (*) in the Fig. 4(a)). These new XRD peaks are identified as belonging to hexagonal ZnO (indexed according to JCPDS No-89-1397). From this study, it is confirmed that the as-deposited film is metallic Zn, whereas the film annealed at 500 °C (morphology C) is a composite of metallic Zn and ZnO. Similar inferences are drawn from the Raman spectra presented in Fig. 4(b). The Raman spectrum of morphology C BSG/Zn film has strong Raman shift at 438 cm^{-1}, which is the characteristic peak of the Wurtzite phase of ZnO(E_2 mode). There are additional weak peaks observed at 324 cm^{-1}, 577 cm^{-1}, and 675 cm^{-1}, which are attributed to the E_{2H}-E_{2L}, E_1(LO), B_1(TA + LA) modes of Wurtzite ZnO phase, respectively.[31] The typical TEM bright field image of morphology C BSG/Zn film is presented in Fig. 4(c). The bright field image has two ZnO nanorods with different diameter. The selected area diffraction (SAED) pattern of this region shows that the diffraction spots are due to hexagonal ZnO. The diffraction spots designated by A, B, and C in Fig. 4(d) have "*d*" values of 0.26 nm, 0.26 nm, and 0.16 nm, respectively, corresponding to the (100), (010), and (1$\bar{1}$0) planes of hexagonal ZnO (according to JCPDS No-89-1397). No signature of diffraction spot from metallic Zn is observed in the SAED pattern. This observation confirms that the nanorods are pure ZnO with no metallic Zn residue. The high resolution TEM image presented in Fig. 4(e) has lattice pattern with $d = 0.25$ nm, which further confirms the (100) planes of the ZnO nanorods. The mechanism of growth of these ZnO nanostructures has been reported earlier.[33] Briefly, when the metallic Zn films are subjected to annealing at 500 °C, which is far beyond the melting point of metallic Zn, i.e., 420 °C, the melting metal plays the role of reactant and catalyst simultaneously. At temperatures above the melting point of Zn, the metal forms molten liquid droplets and oxygen present in the ambient atmosphere get adsorbed on this surface. Thereafter, the molten Zn reacts with the adsorbed oxygen to

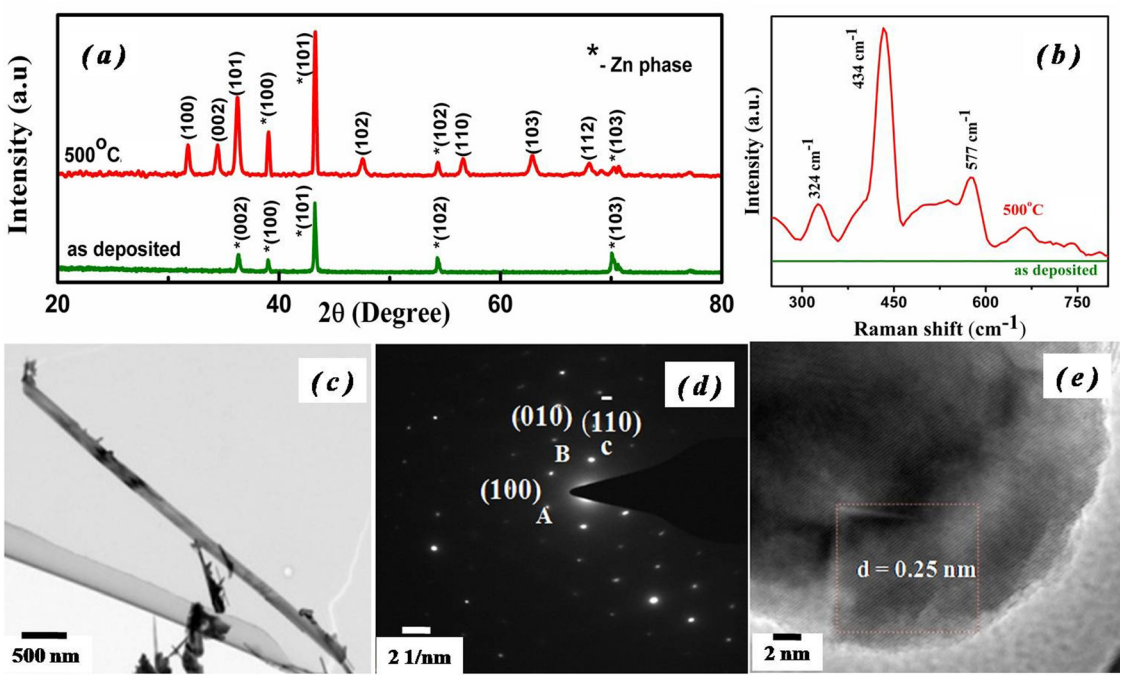

FIG. 4. Characterization data of the ZnO nanostructures: (a) XRD pattern and (b) Raman spectra of BSG/Zn films as-deposited and Morphology C sample. (c) Bright field image, (d) SAED pattern, (e) HRTEM image of BSG/ZnO Morphology C.

form ZnO droplets, which act as nuclei for the formation of dendrites and nanowires.[23] Furthermore, the diffusion of metallic Zn through the newly formed ZnO also controls the growth of nanostructures. The dispersion in dimensions and orientations of the ZnO nanostructures strongly depend on the heat treatment conditions. A variety of nanostructures with different dimensions and orientation are observed in different morphology BSG/ZnO films that are annealed at 500 °C. The thickness of the BSG/Zn film was measured before and after annealing at 500 °C for different morphologies. It was observed that the thickness of the film decreased by 10% (approximately) in all the samples after heat treatment, which may be due to Zn re-evaporation. Similar results were obtained in our previous works.[24] Ivano *et al*. have reported similar growth of chestnut husk-like ZnO starting from Zn powders. The self-catalytic liquid solid growth process of ZnO_{1-x} seed leads to the final architecture made up of ZnO whiskers stemming from ZnO platelets, which were self-assembled into spheroidal agglomerates.[35]

The microstructure of the ZnO/Ag film, shown in the inset of Fig. 2(c), reveals a homogeneous distribution of spherical Ag nanoparticles (~50 nm diameter) decorating the ZnO nanowires. Due to their complex hierarchy, the Ag decorated ZnO nanostructures encompass a large number of plasmon fields, which in turn lead to a large number of hot-spots. The microstructure of BSG/Ag films is presented in the supplementary material S2.[34] The microstructure has ellipsoidal particles with approximate dimensions of the order of 15–20 nm over the entire surface. Closer examination of the microstructure, at higher magnification, demonstrates that the film has discontinuous morphology with relatively larger particle size of the order of 15–20 nm separated by nanoparticles. The growth of such isolated nanostructures is due to the low rate of deposition, which is possible in ion beam sputtering technique. The combination of low energy, low flux, and large substrate distances has led to good control over the nanostructural evolution of the Ag film. Ultra-low ion energy sputter deposition results in very low rates of deposition, which in turn leads to the Ag particles condensing on the substrate with an energy that is much lower than the activation energy barrier for surface diffusion at room temperature.[32] This results in the freezing of the particles without diffusion across the substrate forming discontinuous nanostructured films.

The SERS spectra of Rh6G and ANTA molecules collected over the Ag decorated ZnO nanostructures for different kind of morphologies (A-F) are displayed in Figs. 5(a) and 5(b), respectively. The Ag decorated ZnO nanostructures were able to detect a highly diluted (1 nM) Rh6G molecule in methanol solvent [Fig. 5(a)]. In contrast, the minimum concentration of Rh6G that Ag nanostructures deposited over BSG substrate could detect was 0.1 M as shown in Fig. 5(a). The Raman bands identified in the SERS spectra of Rh6G molecule at 611 cm^{-1}, 773 cm^{-1}, and 1182 cm^{-1}were assigned to C–C–C ring in-plane bending, xanthene skeleton out-of-plane bending motion of the hydrogen atoms, and C–C stretching vibrations, respectively. The bands at 1360 cm^{-1}, 1506 cm^{-1}, and 1647 cm^{-1} are attributed to the aromatic C–C stretching vibrations of Rh6G molecules.[36] The SERS enhancement factor (EF) was calculated using the following formula:[37]

$$\mathrm{EF} = \frac{I_{SERS}}{I_{RS}} \frac{N_{RS}}{N_{SERS}},$$

where I_{SERS} is the enhanced Raman intensity at lower concentration on SERS substrate, I_{RS} is the normal Raman intensity at higher concentration measured over non-plasmon

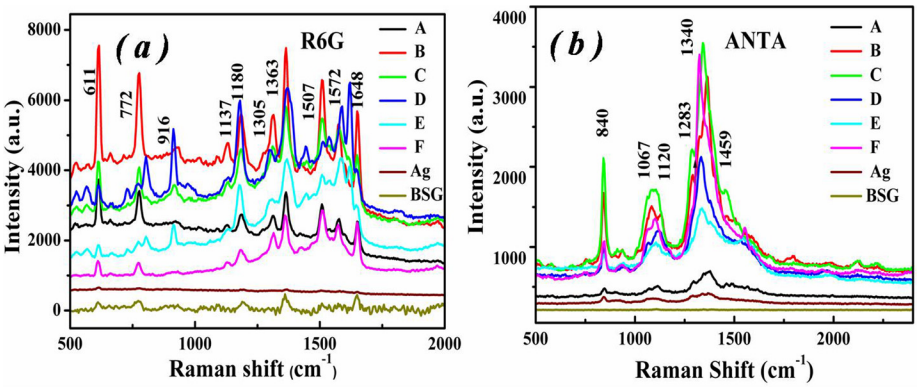

FIG. 5. SERS spectra of (a) Rh6G and (b) ANTA molecule adsorbed on Ag decorated ZnO films (Morphologies A, B, C, D, E, and F).

surface, N_{SERS} is the number of molecules that giving rise to SERS from Ag decorated ZnO nanostructure, N_{RS} is the number of molecules giving rise to Raman signal from non-SERS surface. N_{SERS} and N_{RS} are determined by the relation[38]

$$N_{SERS} = \eta N_A V C_{SERS} \frac{A_{laser}}{A_{SERS}}, \quad N_{RS} = N_A V C_{RS} \frac{A_{laser}}{A_{RS}},$$

where η is the adsorption factor, N_A is Avogadro number, V is total volume of the solution added onto the substrate, A_{laser} is the area of the laser spot, A_{SERS} and A_{RS} are the total area of the SERS and non-SERS substrate, respectively, C_{SERS} and C_{RS} are the lower and higher concentration of analyte applied over SERS and non-SERS substrates, respectively. The adsorption factor (η) was estimated following the Langmuir isotherm models[39,40] as described in our previous reports.[38,41] The detail of the adsorption factor calculation is reported in the supplementary material S3.[34] The area under the Raman peak centered around 1362 cm^{-1} has been chosen for EF calculation of ZnO/Ag samples annealed at 500 °C for different morphologies (A to F), and the calculated values are 5×10^8, 1.5×10^9, 9.7×10^8, 3.1×10^9, 2.2×10^9, and 4.7×10^8, respectively. The corresponding EF values for Ag nanostructures deposited on BSG substrate is 4.6×10^6.

The SERS spectra of the ANTA molecule in acetonitrile (0.1 M for non-resonant Raman and 10 μM concentration for SERS) presented in Fig. 5(b) exhibit strong characteristic Raman modes at 840 cm^{-1}, 940 cm^{-1}, 1120 cm^{-1}, 1283 cm^{-1}, 1340 cm^{-1}, and 1459 cm^{-1}. These Raman modes are assigned to NO_2 deformation + ring deformation (840 cm^{-1}), ring deformation (1067 cm^{-1}), N-N symmetric stretch (1120 cm^{-1}), ring deformation +N-H bend (1283 cm^{-1}), C-NO_2 symmetric stretch (1340 cm^{-1}), and C-N symmetric stretch (1459 cm^{-1}).[38] The strong Raman peak in the vicinity of 1340 cm^{-1} has been selected for EF calculation for ANTA molecule, and the values for different morphologies (A-F) are 9.6×10^6, 3.3×10^7, 7.1×10^7, 2.6×10^7, 1.7×10^7, and 5.4×10^7, respectively. In comparison, the EF was only 1.1×10^4 for the Ag nanostructures on BSG. Three orders higher EF is recorded for ZnO/Ag 3-D nanostructures relative to their BSG/Ag nanostructure counterparts. Reproducibility is one of the essential parameters to establish feasibility of these SERS substrates for practical applications. The SERS signal was collected from 20 different sites on the morphology F ZnO/Ag sample, to establish reproducibility. The SERS spectra for ANTA collected from different sites along with the corresponding enhancement factor using the Raman peak at 1340 cm^{-1} are depicted in Figures 6(a) and 6(b), respectively. The relative standard deviation (RSD) of SERS intensity for 20 different sites on the same sample is 28%, whereas that for BSG/Ag substrate is 34%. The relatively smaller RSD suggests that the ZnO/Ag 3D nanostructure is more suitable as a SERS detection probe in comparison to the BSG/Ag 2D structure.

The SERS spectra of two other explosive molecules, FOX-7 and CL-20, recorded using the same method over ZnO/Ag nanostructures produced by annealing the Zn film at different morphologies are compared in the Figures 7(a) and 7(b), respectively. The two most prominent peaks in the SERS spectra of FOX-7, in Fig. 7(a), are assigned to the C-NO_2 bend (860 cm^{-1}) and skeletal deformation (1339 cm^{-1}) modes, respectively.[42] The additional modes observed in the Raman spectra also match with previous reports.[43] EFs were calculated based on the change in area under the skeletal

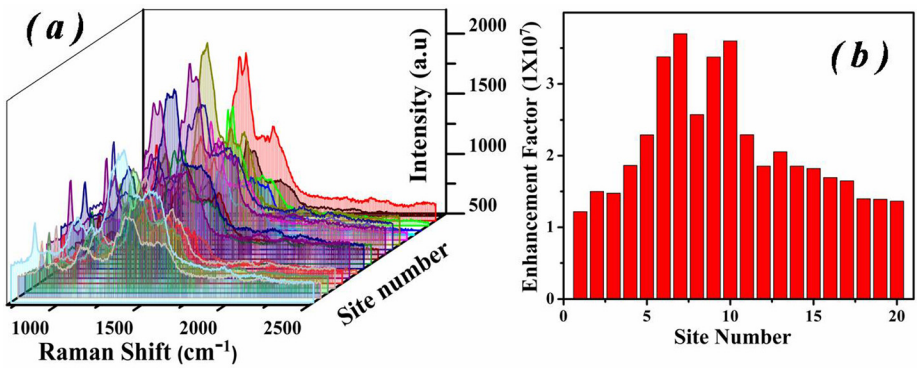

FIG. 6. (a) SERS spectra of ANTA analyte and its (b) enhancement factor collected at 20 different sites over Ag/ZnO morphology C sample.

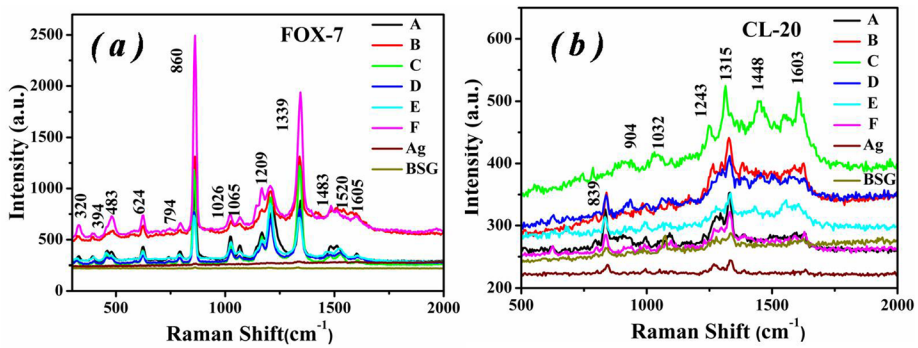

FIG. 7. SERS spectra of (a) FOX-7 and (b) CL20 molecule adsorbed on Ag decorated ZnO films (Morphologies A, B, C, D, E, and F).

deformation Raman mode at 1339 $cm^{-1}$for different morphology (A-F) ZnO/Ag films, and the values are 7.4×10^6, 1.0×10^7, 1.3×10^7, 6.2×10^6, 5.3×10^6, and 1.8×10^7, respectively. In contrast, the EF value is only 1.5×10^4 for the Ag nanostructure deposited directly on the BSG substrate. The observed peaks in the SERS spectra of CL-20 shown in Fig. 7(b) at 832 cm^{-1} are assigned to O-N-O bending; 904 cm^{-1} and 1032 cm^{-1} to NN-stretching; 1243 cm^{-1}, 1315 cm^{-1}, and 1448 cm^{-1} to CH bend; and 1603 cm^{-1} to the asymmetric NO_2 stretching band.[44,45] EFs are calculated for the most intense peak at 1315 cm^{-1}, and the values are 3.2×10^4, 2.6×10^4, 3.4×10^4, 2.3×10^4, 1.42×10^4, and 2.1×10^4 for different morphology Ag decorated ZnO (A to F, respectively) films produced by annealing Zn film at 500 °C, respectively. The EF for the Ag nanostructure deposited directly on BSG substrate is much lower (three times).

Two major observations can be concluded from the results presented in Figs. 2–7: (1) there is a major change in the microstructure of the ZnO films with change in dwell times at 500 °C and (2) the Ag decorated ZnO nanostructures are more sensitive to the presence of explosive molecules than Ag deposited directly on the BSG substrates. The enhancement factor for ZnO/Ag nanostructures of different morphology (A-F) and BSG/Ag microstructures for different SERS analytes are compared in Fig. 8. It is pertinent to note

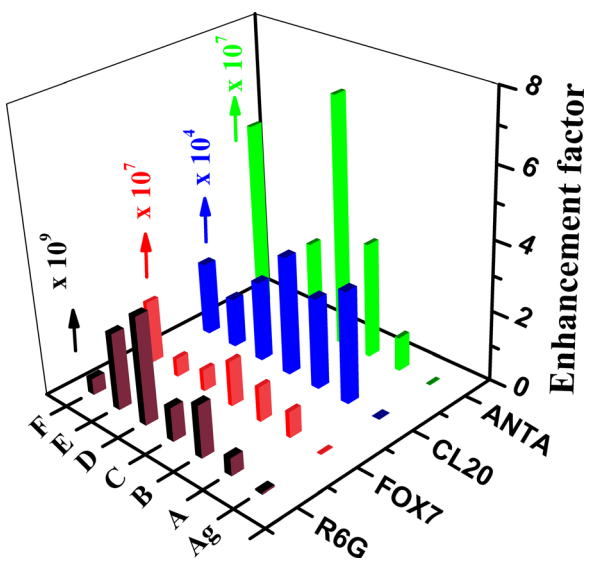

FIG. 8. Enhancement factors for different Ag/ZnO probes (Morphologies A, B, C, D, E, and F) along with BSG/Ag for Rh6G and different high energy molecules. The highest EF was observed for Rh6G molecule.

that deposition of Ag on BSG and ZnO nanowires is carried out at the same time. Hence, conditions of deposition are exactly same in both cases. The reasons for the difference in sensitivity in the two cases are now examined. The increase in the sensitivity of the SERS signal detection in ZnO/Ag can, to a first approximation, can be attributed to the high density of hot spots[13] that the three dimensionally (3-D) networked nanostructure of ZnO nanowires provides. These Ag decorated 3-D nanostructured surfaces provide large surface area for adsorbing the probe molecules, and localized surface plasmons of Ag on the spatially arranged mosaic nanostructures enhance the local electric fields to generate extremely large hot-spots.[12] Furthermore, internal scattering of transmitted photons at nano-voids in the Ag decorated ZnO nanostructures leads to improved quantum yields and greater sensitivity for molecular detection by SERS.[12] Lahiri *et al.* have reported an enhanced SERS effect on Au/Si heterojunctions derived from the electron transfer from semiconductor (Si) to metal (Au) through the interface.[46] In the present case, the surrounding semiconductor (ZnO) has metal residue (Zn), which facilitates the electron transfer from semiconductor to Ag. The presence of Zn metal residue in the ZnO/Ag nanostructure is confirmed through XRD studies. The X-ray diffraction pattern of Zn film annealed at 500 °C for different morphology (A-F) followed by 10 nm Ag film decoration is shown in Fig. 9. The XRD pattern shows that the films are polycrystalline in nature, and there are contributions from both hexagonal ZnO and metallic Zn (confirmed from JCPDS card nos. 89–1397 and 87–0713, respectively). Significantly, no diffraction peaks from metallic Ag are observed. However, the presence of Ag is

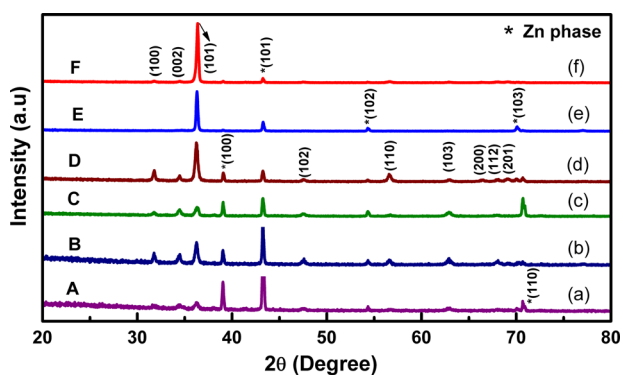

FIG. 9. X-ray diffraction patterns of Zn film annealed at 500 °C for different morphologies A, B, C, D, E, and F.

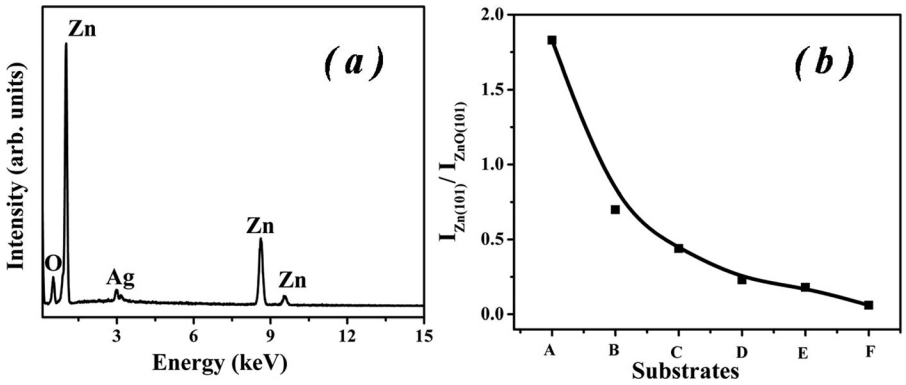

FIG. 10. (a) EDS spectra of Ag/ZnO nanostructure. (b) Variation in the ratio of XRD peak intensity Zn (101) and ZnO (101) as a function of different morphology samples.

confirmed through EDS, as shown in Fig. 10(a). It is evident from a calculation of the ratio of the area under the strong XRD peaks[47] of Zn (101) and metallic ZnO (101) that the Zn residue content decreases from morphology A to F as shown in Fig. 10(b). From this, it is inferred that the amount of Zn metal residue in the ZnO matrix depends on dwell times. In general, the chemical enhancement contribution in SERS is attributed to the charge interactions between the absorbed molecules and noble metal (Ag) structures. In semiconductor assisted SERS, the enhancement is attributed to the charge transfer between semiconductor nanoparticles and the molecule under investigation.[48] Due to this reason, nano-dimensional semiconductor structures have been demonstrated to exhibit effective SERS enhancements,[48] which is expected to be true even in the case of Ag decorated ZnO nanowires of the present study. In the present case, we expect that the metallic Zn in ZnO nanostructures may lead to enhanced electron charge transfer from the semiconductor (ZnO) and Ag to probe molecule, which in turn affects the SERS enhancement. In our recent work, we have demonstrated that the body of the nanowire is purely made of ZnO, and the base has metallic Zn component.[49] The metallic Zn and decorating Ag nanoparticles are, thus, shielded by the semiconductor ZnO nanostructure. The dimensions of nanostructure (length, width, and orientation) are expected to determine the extent of influence of metallic Zn on the chemical shift effect and semiconductor SERS effect. Alessandri *et al.* has presented a non-plasmon assisted SERS

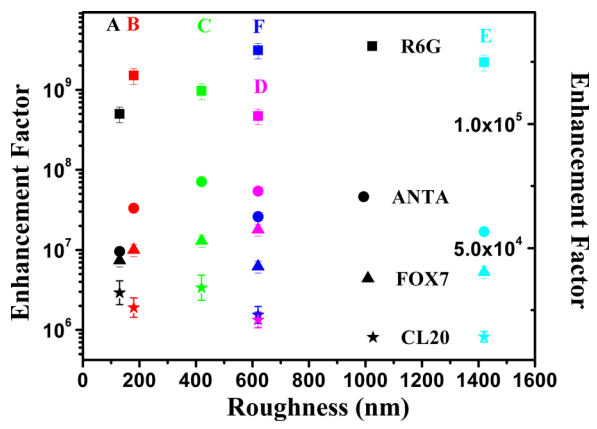

FIG. 11. Quantitative comparison of enhancement factor for different analytes with varying roughness of the ZnO film.

enhancement in TiO_2 based spherical resonators. The extraordinary scattering of the exciting light due to internal reflections in titania shell layer has resulted to enhanced Raman signals.[50] Dikovska *et al.* reported that the intensity of SERS signal drops with increasing dimensions of nanostructure due to the higher density of spatial inhomogeneities that will survive in the smallest dimension nanostructures.[51] N. Bontempi *et al.* have compared the relation between the light trapping capabilities of Si nanowires with SERS enhancement in high density Si nanowire arrays obtained by electroless etching.[52] This phenomenon is molecule and nanostructure dependent. In the present case, the nanostructure formed is dwell time dependent. As a consequence, the highest EF for different molecules does not occur either at the same morphology or same concentration. The quantitative comparison of EF versus PPH for different analytes is presented in Fig. 11. It is observed that the EF is independent of the huge change in the morphology of the sample (from 100 nm to 1450 nm). No systematic variation of EF is observed with PPH of different morphologies: A to F. On the other hand, the observed changes in EF may be solely ascertained to the Zn metal residue present in the samples. From this study, we conclude that the SERS with higher detection sensitivity can be achieved by depositing Ag discontinuous layer on the ZnO mosaic microstructure. Our future studies will comprise the detection of other common explosive molecules such as ammonium nitrate. Our efforts will also be focused on (a) achieving higher sensitivity, (b) investigating the reusability of the same substrate[38] for detecting different molecules by utilizing other plasmonic metals (e.g., Au and Cu[52]), and (c) exploring the utility of such structures for SERS based detection in other fields (e.g., drugs and cancer).[52]

IV. CONCLUSIONS

In conclusion, trace level detection of explosive molecules utilizing the ZnO/Ag 3D nanostructures has been successfully demonstrated. Different ZnO nanostructures were realized by the thermal oxidation of precursor Zn films at 500 °C. The Ag decorated ZnO nanostructure exhibited higher sensitivity and three orders of magnitude higher SERS enhancement than the same Ag nanostructure deposited directly on BSG substrate. This enhancement is successfully utilized in trace level detection of three explosive molecules, namely, ANTA, CL-20, and FOX-7.

ACKNOWLEDGMENTS

The authors acknowledge the financial support from DRDO, India, and the facilities provided by Centre for Nanotechnology and School of Physics, University of Hyderabad, India, under the UGC-CAS, UPE programs. U.P.S. acknowledges ACRHEM for fellowship support during this work. Md. A.M. acknowledges SERB for the project SB/FTP/PS049/2014. S. Venugopal Rao acknowledges partial financial support from UPE-2, University of Hyderabad.

[1]C. Wynn, B. Edwards, R. Kunz, J. Zayhowski, S. Palmacci, and M. Rothschild, SPIE Newsr. (2008).
[2]Z. Bielecki, J. Janucki, A. Kawalec, J. Mikolajczyk, N. Palka, M. Pasternak, T. Pustelny, T. Stacewicz, and J. Wojtas, Metrol. Meas. Syst. **19**, 3 (2012).
[3]A. Hakonen, P. O. Andersson, M. Stenbaek Schmidt, T. Rindzevicius, and M. Käll, Anal. Chim. Acta **893**, 1 (2015).
[4]H. Zhou, Z. Zhang, C. Jiang, G. Guan, K. Zhang, Q. Mei, R. Liu, and S. Wang, Anal. Chem. **83**, 6913 (2011).
[5]S. K. Jha, Y. Ekinci, M. Agio, and J. Löffler, Analyst **140**, 5671 (2015).
[6]M. Terakawa, S. Takeda, Y. Tanaka, G. Obara, T. Miyanishi, T. Sakai, T. Sumiyoshi, H. Sekita, M. Hasegawa, P. Viktorovitch, and M. Obara, Prog. Quantum Electron. **36**, 194 (2012).
[7]S. Maier and H. Atwater, J. Appl. Phys. **98**, 011101 (2005).
[8]S. K. Ghosh and T. Pal, Chem. Rev. **107**, 4797 (2007).
[9]D. Lis and F. Cecchet, Beilstein J. Nanotechnol. **5**, 2275 (2014).
[10]G. Sinha, L. E. Depero, and I. Alessandri, ACS Appl. Mater. Interfaces **3**, 2557 (2011).
[11]M. Zhou, K. Diao, J. Zhang, and W. Wu, Phys. E **56**, 59 (2014).
[12]Y. Chen, G. Tian, K. Pan, C. Tian, J. Zhou, W. Zhou, Z. Ren, and H. Fu, Dalton Trans. **41**, 1020 (2012).
[13]X. He, H. Wang, Q. Zhang, Z. Li, and X. Wang, Eur. J. Inorg. Chem. **2014**, 2432.
[14]A. Musumeci, D. Gosztola, T. Schiller, N. M. Dimitrijevic, V. Mujica, D. Martin, and T. Rajh, J. Am. Chem. Soc. **131**, 6040 (2009).
[15]P. Xu, N. H. Mack, S. H. Jeon, S. K. Doom, X. Han, and H. L. Wang, Langmuir **26**, 8882 (2010).
[16]L. Sun, D. Zhao, Z. Song, C. Shan, Z. Zhang, B. Li, and D. Shen, J. Colloid Interface Sci. **363**, 175 (2011).
[17]K. Liu, M. Sakurai, M. Liao, and M. Aono, J. Phys. Chem. C **114**, 19835 (2010).
[18]M. Macias-montero, V. J. Rico, Z. Saghi, P. Midgley, C. N. Afonso, R. Gonza, and A. Borras, ACS Appl. Mater. Interfaces **7**, 2331 (2015).
[19]M. Gao, G. Xing, J. Yang, L. Yang, Y. Zhang, H. Liu, H. Fan, Y. Sui, B. Feng, Y. Sun, Z. Zhang, S. Liu, S. Li, and H. Song, Microchim. Acta **179**, 315 (2012).
[20]A. E. Kandjani, M. Mohammadtaheri, A. Thakkar, S. K. Bhargava, and V. Bansal, J. Colloid Interface Sci. **436**, 251 (2014).
[21]K. Sivashanmugan, J.-D. Liao, B. H. Liu, C.-K. Yao, and S.-C. Luo, Sens. Actuators, B **207**, 430 (2015).
[22]X. Li, G. Chen, L. Yang, Z. Jin, and J. Liu, Adv. Funct. Mater. **20**, 2815 (2010).
[23]H. S. Gill, S. Thota, L. Li, H. Ren, R. Mosurkal, and J. Kumar, Sens. Actuators, B **220**, 794 (2015).
[24]U. P. Shaik, S. Kshirsagar, M. G. Krishna, S. P. Tewari, D. Dhar Purkayastha, and V. Madhurima, Mater. Lett. **75**, 51 (2012).
[25]H. W. Kang, J. Leem, and H. J. Sung, RSC Adv. **5**, 51 (2015).
[26]H. He, H. Li, W. Xia, X. Shen, M. Zhou, J. Han, X. Zeng, and W. Cai, J. Mater. Chem. C **3**, 1724 (2015).
[27]Q. Tao, S. Li, C. Ma, K. Liu, and Q.-Y. Zhang, Dalt. Trans. **44**, 3447 (2015).
[28]C. Zhu, G. Meng, Q. Huang, X. Wang, Y. Qian, X. Hu, H. Tang, and N. Wu, Nano Res. **8**, 957 (2015).
[29]X. He, H. Wang, Z. Li, D. Chen, and Q. Zhang, Phys. Chem. Chem. Phys. **16**, 14706 (2014).
[30]S. D. Kshirsagar, U. Pasha Shaik, M. G. Krishna, and S. P. Tewari, J. Lumin. **136**, 26 (2013).
[31]U. P. Shaik, P. A. Kumar, M. G. Krishna, and S. V. Rao, Mater. Res. Express **1**, 046201 (2014).
[32]R. Brahma and M. G. Krishna, Phys. E **43**, 1192 (2011).
[33]U. P. Shaik and M. G. Krishna, Ceram. Int. **40**, 13611 (2014).
[34]See supplementary material at http://dx.doi.org/10.1063/1.4943034 for cross-sectional roughness in AFM, FESEM image of Ag decorated BSG substrate and detailed Enhancement factor calculations.
[35]I. Alessandri, P. Bergese, and L. E. Depero, J. Nanosci. Nanotechnol. **9**, 1597 (2009).
[36]L. Jensen and G. C. Schatz, J. Phys. Chem. A **110**, 5973 (2006).
[37]M. A. Mohiddon, L. D. V. Sangani, and M. G. Krishna, Chem. Phys. Lett. **588**, 160 (2013).
[38]S. Hamad, G. K. Podagatlapalli, A. Mohiddon, and V. R. Soma, Appl. Phys. Lett. **104**, 2631041 (2014).
[39]N. Ahalya, R. Kanamdi, and T. V. Ramachandra, Indian J. Chem. Technol. **13**, 122 (2006).
[40]K. R. Hall, L. C. Eagleton, A. Acrivos, and T. Vermeulen, I&EC Fundam. **5**, 212 (1966).
[41]G. K. Podagatlapalli, S. Hamad, and V. R. Soma, J. Phys. Chem. C **119**, 16972 (2015).
[42]S. Hamad, G. Krishna Podagatlapalli, M. Ahamad Mohiddon, and S. Venugopal Rao, Chem. Phys. Lett. **621**, 171 (2015).
[43]D. C. Sorescu, J. A. Boatz, and D. L. Thompson, J. Phys. Chem. A **105**, 5010 (2001).
[44]Y. Kholod, S. Okovytyy, G. Kuramshina, M. Qasim, L. Gorb, and J. Leszczynski, J. Mol. Struct. **843**, 14 (2007).
[45]G. K. Podagatlapalli, S. Hamad, M. A. Mohiddon, and S. V. Rao, Laser Phys. Lett. **12**, 036003 (2015).
[46]A. Lahiri, R. Wen, S. Kuimalee, S. Kobayashi, and H. Park, CrystEngComm. **14**, 1241 (2012).
[47]M. A. Mohiddon and K. L. Yadav, Adv. Appl. Ceram. **107**, 310 (2008).
[48]S. Hamad, P. G. Krishna, M. A. Mohiddon, and S. V. Rao, Appl. Phys. Lett. **104**, 263104 (2014).
[49]U. P. Shaik and M. G. Krishna, AIP Conf. Proc. **1591**, 405 (2013).
[50]I. Alessandri, J. Am. Chem. Soc. **135**, 5541 (2013).
[51]A. O. Dikovska, N. N. Nedyalkov, S. E. Imamova, G. B. Atanasova, and P. A. Atanasov, Quantum Electron. **42**, 258 (2012).
[52]N. Bontempi, M. Salmistraro, M. Ferroni, L. E. Depero, and I. Alessandri, Nanotechnology **25**, 465705 (2014).